Deformation and damping behaviours of microcrystalline Mg reinforced with ceramic nanoparticles

P. Lukáč*, Z. Trojanová

Charles University, Faculty of Mathematics and Physics, Department of Metal Physics, Ke Karlovu 5, 121 16 Prague 2, Czech Republic

Received 8 August 2006, received in revised form 19 September 2006, accepted 5 October 2006

Abstract

The Mg micropowders were atomised with argon. Various ceramic and carbon nanoparticles were generated by laser-induced gas phase reaction in a flow reactor. The Mg powders were mixed or ball milled with nanoscaled particles and hot extruded. The deformation behaviour of the nanocomposites was investigated by tensile or compression tests at different temperatures at a constant initial strain rate. The test temperature significantly influences the flow stress. The damping was measured as the logarithmic decrement of the free decay of the vibrating beam of the composite. The volume fraction and the kind of the reinforcement influence the value of the logarithmic decrement and its strain amplitude dependence. A high damping is observed.

K e y w o r d s: magnesium, composites, mechanical properties, damping

1. Introduction

Magnesium alloys have the lowest density of metallic materials, which can be considered for many structural applications. Owing to their low density they exhibit a high specific strength (the strength/density ratio) and a high specific stiffness. However, the yield stress and tensile strength of magnesium alloys are very sensitive to temperature [1–5]. The strength of magnesium alloys can be improved by solid solution hardening, precipitation and dispersion strengthening [6]. Grain size refinement methods have been successfully used in the attempt to increase the strength of magnesium alloys [7–10]. An increase of the yield stress σ_y with decreasing grain size d may be described by the Hall-Petch relationship [11, 12]

$$\sigma_y = \sigma_0 + k_y d^{-1/2}, \quad (1)$$

where σ_0 and k_y are constants. The elongation to fracture in Mg alloys increases with decreasing grain size. The Hall-Petch relationship in some nanocrystalline Mg alloys is not valid below a certain grain size [10]. Deformation mechanisms may change with a decrease in grain size. Thus, grain boundary sliding is the deformation mechanism of nanocrystalline magnesium deformed in compression at room temperature [13]. On the other side, Suryanarayana [14] claimed that ultrafine-grained materials, with grain sizes between 100 and 1000 nm, have the greatest potential for industrial applications.

The addition of reinforcement, fibres and/or particulates, increases the strength of Mg and its alloys. Mechanical properties of Mg composites are strongly dependent on the type, size and distribution of reinforcements [15, 16]. The microstructure of Mg-based composites is sensitive to thermo-mechanical treatments, thermal cycling and changes in temperature. Internal thermal stresses may be generated and they influence not only the mechanical properties but also physical properties such as the coefficient of thermal expansion and damping [17].

It is expected that new promising materials may be produced when nanosized ceramic particles are added and distributed in Mg matrices with fine or ultrafine grains. These Mg-based nanocomposites may be fabricated by mixing and co-milling of microscaled metal powder with nanoscaled particles followed by hot consolidations [18, 19] or by friction stir processing [20]. Very recently we have presented the influence of

*Corresponding author: tel.: +420 221911366; fax: +420 221911490; e-mail address: lukac@met.mff.cuni.cz

ceramic nanoparticles and graphite on the mechanical properties of microcrystalline and ultrafine-grained magnesium [21, 22]. The composites have low density and a relatively high strength and damping. The damping behaviour may be determined using resonant experiments when the decay of free vibrations of the system is measured after excitation [23]. The logarithmic decrement δ, which expresses the reduction in amplitude of a freely decaying system during one cycle, is defined as

$$\delta = \ln(A_n/A_{n+1}), \tag{2}$$

where A_n and A_{n+1} are the amplitudes of a free decay of vibrations after n cycles and $(n + 1)$ cycles, respectively. Measurement of δ at low strains (stresses) is a sensitive method determining the microstructure of the material and changes in the microstructure.

Based on a literature review, the aim of the present paper is to explain the effect of the presence of different types of nanoparticles on the deformation and damping behaviour of magnesium.

2. Materials and experimental procedure

Materials used in this study were ultrafine-grained Mg (hereafter UFG-Mg), UFG-Mg reinforced with 3 vol.% of graphite, microcrystalline Mg (hereafter μ-Mg), μ-Mg with 1 and 3 vol.% of Al_2O_3 nanoparticles, μ-Mg reinforced with 3 vol.% of ZrO_2 and of SiC nanoparticles. The microscaled Mg powders (with a median particle size of about 20 μm) were prepared by gas atomisation of a high purity Mg melt with argon atmosphere containing 1 % oxygen for powder passivation. Al_2O_3, ZrO_2 and SiC powders with a mean particle size of 14 nm were prepared by evaporation with the pulsed radiation of a 1000 W Nd: YAG laser and subsequent condensation of the laser-induced vapour in a controlled aggregation gas. The preparation method of nanoparticles is described elsewhere [18, 19]. Mg powders were mixed with ceramic nanoparticles in an asymmetrically moved mixer for 8 h. The powder mixture was then milled together for 1 h in a planetary ball mill. The mixture was subsequently precompacted, degassed and hot extruded at a temperature of 350 ℃ under a pressure of 150 MPa. The grain size after extrusion was in the cross-section about 3 μm and in the extrusion direction 10 μm.

Ultrafine-grained Mg specimens were prepared by ball milling procedure in an inert atmosphere and subsequently consolidated and hot extruded. The Mg powder was mixed with 3 vol.% of 99.9 % pure graphite powder in an asymmetrically moving mixer for 8 h. The mixtures were then milled for 8 h at 200 rpm in a planetary ball mill in a sealed argon atmosphere. The preparation method of UFG-Mg reinforced with graphite nanoparticles is described elsewhere [22, 24]. The mean grain size of specimens estimated using transmission electron microscopy and X-ray line profile analysis was about 200 nm.

Tensile tests were performed in an Instron testing machine at temperatures between 20 and 300 ℃ at a constant crosshead speed giving an initial strain rate of 6.2×10^{-5} s^{-1}. Uniaxial compression tests were carried out at a constant crosshead speed giving an initial strain rate of 1.4×10^{-4} s^{-1}. The testing temperature in a furnace was controlled to $\pm$ 1 ℃. Testing specimens were machined from the extruded bars with their symmetry axis parallel to the extrusion direction. The yield stress σ_{02} was determined as the flow stress at 0.2% strain and the maximum stress σ_{m} as the maximum value of the flow stress. The elongation to fracture was determined in the tensile tests.

Damping measurements were carried out on bending beams (81 mm long, 10 mm wide with thickness of 4 mm) fixed at one end in a vacuum at room temperature. Damping was measured as the logarithmic decrement δ of the vibrating beam. Measurements of the strain amplitude dependences of the logarithmic decrement are described elsewhere [25]. The specimens were annealed step by step at increasing temperatures for 0.5 h and after each annealing cycle quenched into water at room temperature. The damping measurements were performed immediately.

3. Experimental results and discussion

3.1. Mechanical properties and deformation behaviour

Figure 1 shows the true stress-true strain curves of ultrafine-grained magnesium deformed in compression [26]. Specimens were deformed either to fracture or at higher temperatures to predetermined strains (about 0.25), to which deformation can be considered as homogeneous. A pronounced upper yield point followed by softening and then by the hardening stage was observed at the beginning of deformation at temperatures between room temperature and 100 ℃. The true stress-true strain curves measured at temperatures higher than 100 ℃ have a steady state character – without hardening. Flow stress decreases very rapidly with increasing temperature. A high dislocation density accumulated during preparation of specimens by milling is partly recovered during consolidation and hot extrusion. An upper yield point at the beginning of deformation at lower temperatures is very probably caused by the avalanche release of dislocations pinned at grain boundaries. At temperatures above 100 ℃, there is a dynamic balance between harden-

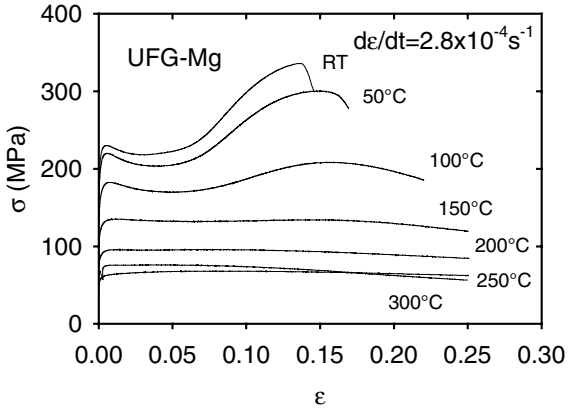

Fig. 1. True stress-true strain curves obtained for ultrafine-grained Mg.

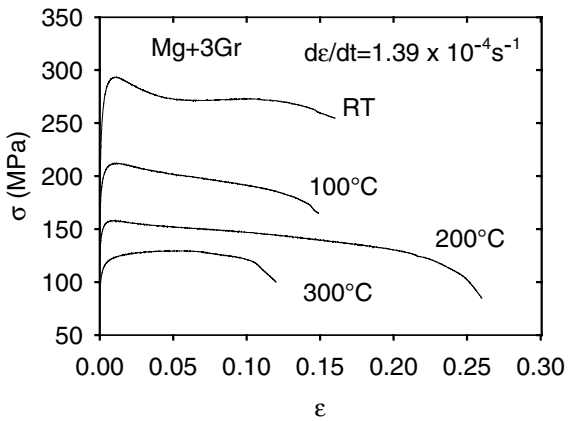

Fig. 2. True stress-true strain curves for ultrafine-grained Mg reinforced with 3 vol.% of graphite nanoparticles.

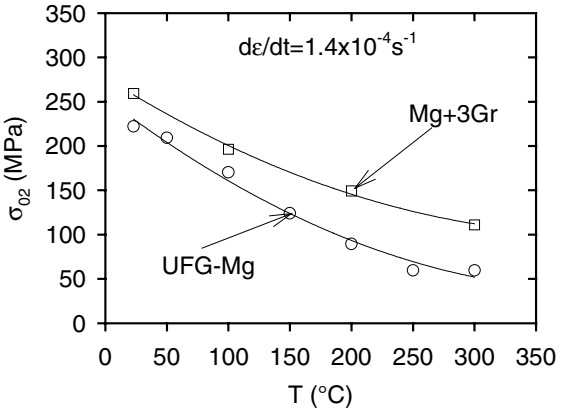

Fig. 3. Temperature dependences of the yield stress for ultrafine-grained Mg and ultrafine-grained Mg reinforced with 3 vol.% of graphite nanoparticles.

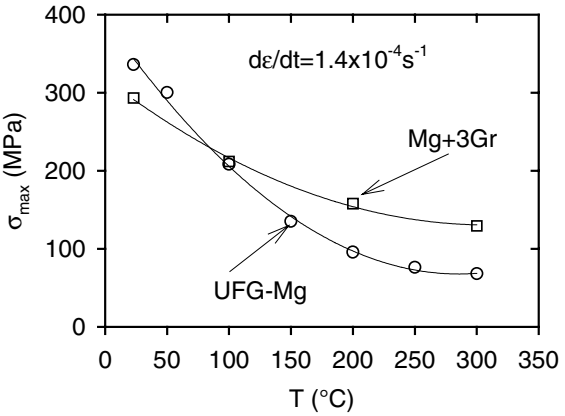

Fig. 4. Temperature dependences of the maximum stress for ultrafine-grained Mg and ultrafine-grained Mg reinforced with 3 vol.% graphite nanoparticles.

ing and softening. Dislocations generated reach very rapidly grain boundaries where their annihilation occurs. The average grain size of about 100 nm means that the volume fraction of the grain boundaries is high. The grain boundaries serve as diffusion paths. A temperature of 150 ℃ (about 0.45 T_m, T_m is the melting point) is relatively high. Therefore grain boundary sliding can be expected.

Figure 2 shows the true stress-true strain curves of UFG-Mg reinforced with 3 vol.% graphite nanoparticles deformed in compression [22]. It can be seen that the flow stress decreases with an increase in the testing temperature. At and above 100 ℃, the work hardening rate decreases slowly with strain indicating a softening process. The temperature dependences of the yield stress (σ_{02}) and maximum stress (σ_{max}) obtained for UFG-Mg and UFG-Mg + 3 vol.% Gr are presented in Figs. 3 and 4, respectively.

Specimens of microcrystalline magnesium reinforced with ZrO_2 and Al_2O_3 were deformed in tension [21]. The true stress-true strain curves have a similar shape as those for UFG-Mg reinforced with graphite. At temperatures above 100 ℃, the work hardening rate is close to zero; a dynamic balance between hardening and softening. The flow stresses for μ-Mg+3n-Al_2O_3 are higher than those for μ-Mg+3n-ZrO_2 at the same testing temperature. Figure 5 shows the temperature variation of the yield stress for microcrystalline Mg reinforced with zirconia and alumina nanoparticles. The difference in the yield stress between both materials deformed at room temperature is about 100 MPa, whereas the differences in the yield stress values at and above 200 ℃ are small. On the other hand, the elongation to failure of μ-Mg+3n-ZrO_2 is higher than that of μ-Mg+3n-Al_2O_3. Similar dependences of the yield stress on the testing temperature were observed for μ-Mg and in μ-Mg+1n-Al_2O_3 [27].

Recently, Ferkel and Mordike [28] have reported the deformation behaviour of microcrystalline Mg re-

Table 1. Mechanical properties of Mg reinforced with nanoparticles (in vol.%)

Material	d (μm)	YS (MPa)	UTS (MPa)	ε_f (%)	References
Mg	60 ± 10	132	193	4.2	29
Mg/0.22Al_2O_3	61 ± 18	169	232	6.5	29
Mg/0.66Al_2O_3	63 ± 16	191	247	8.8	29
Mg/1.11Al_2O_3	31 ± 13	194	250	6.9	29
Mg/1.1Al_2O_3 (1.0 μm)	11 ± 3	172	227	16.8	30
Mg/1.1Al_2O_3 (0.3 μm)	11 ± 4	182	237	12.1	30
Mg/1.1 Al_2O_3 (50 nm)	31 ± 13	194	250	6.9	30, 31
Mg/1.1Y_2O_3 (29 nm)	12 ± 3	153	195	9.1	31
Mg/1.1.ZrO_2 (29–68 nm)	11 ± 3	146	199	10.8	31

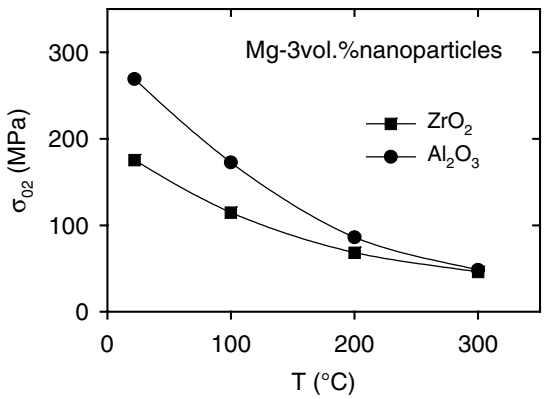

Fig. 5. Temperature dependence of the yield stress of microcrystalline Mg reinforced with 3 vol.% of ZrO_2 and Al_2O_3 nanoparticles.

inforced with 3 vol.% SiC nanoparticles (with a median diameter of 30 nm). The values of the maximum stress at room temperature and 100 ℃ lie between the values of the maximum stress obtained for μ-Mg+3n-ZrO_2 and μ-Mg+3n-Al_2O_3. The values of the maximum stress of Mg+3n-SiC nanoparticles determined at 200 and 300 ℃ are very close to those obtained for μ-Mg+3n-ZrO_2 and μ-Mg+3n-Al_2O_3. Very recently, Hassan and Gupta [29] have reported the room temperature mechanical properties of Mg reinforced with 0.22, 0.66 and 1.11 vol.% of Al_2O_3 nanoparticles (an average size of 50 nm). The addition of 0.22, 0.66 and 1.11 Al_2O_3 nanoparticles to Mg leads to the yield stress of 169, 191 and 194 MPa. Hassan and Gupta [30] investigated effect of length scale of Al_2O_3 particles on tensile properties of magnesium deformed at room temperature. The yield stress increases with decreasing particle size. Hassan and Gupta [31] have also shown that the presence of 1.1 vol.% of different types of nanoparticles (ZrO_2, Y_2O_3, Al_2O_3 – average size of 29–68, 29, 50 nm, respectively) leads to a significant increase in the yield stress and the maximum stress. They found that Al_2O_3 particles were most effective in increasing strength while ZrO_2 nanoparticles were most effective in increasing ductility, which is in agreement with our observation. For the sake of clarity, their results concerning the mechanical properties are given in the Table 1. The 0.2% yield strength (YS), ultimate tensile stress (UTS), ductility (ε_f) and grain size (d) are presented. The results revealed that the yield stress and UTS values of Mg with 0.66 and 1.11 vol.% of Al_2O_3 nanoparticles are higher than those for magnesium without nanoparticles. It is obvious that a decrease in size of Al_2O_3 particles causes an increase in the yield stress and UTS.

The particles in a composite may cause an increase in the dislocation density as a result of thermal strain mismatch between the ceramic particles and the matrix during preparation and/or thermal treatment. The difference between the coefficients of thermal expansion (CTE) of the particles and the matrix may create the thermal residual stresses after cooling from the processing temperature to room temperature. The CTE of the Mg matrix is much higher than that of the ceramic particles and graphite particles. The thermal stresses may relax around the matrix-particle interface by emitting dislocations. An increase in the dislocation density near reinforcement has been calculated as [32, 33]

$$\Delta\rho = \frac{B\, f\, \Delta\alpha\, \Delta T}{b\,(1-f)}\,\frac{1}{t}, \tag{3}$$

where $\Delta\alpha$ is the difference of CTE between matrix and reinforcement, ΔT is a temperature change, t is the minimum size of reinforcement, f is the volume fraction of reinforcement, b is the magnitude of the Burgers vector of dislocations and B is a geometrical constant (depending on the aspect ratio). The newly formed dislocations are obstacles for the motion of dislocations in the matrix. Therefore a higher stress for the moving dislocations is necessary in comparison to magnesium without nanoparticles.

An increase in the yield stress (compared to unreinforced magnesium) can be attributed to the dislocation density increase due to the difference in coefficient of thermal expansion between the particles and Mg matrix. The density of the newly created dislocations increases with an increase in the volume fraction

(using Eq. (3)), which is observed in experiment [29]. An increase in the yield stress with decreasing size of Al_2O_3 particles [30] may be also explained using Eq. (3). The density of the dislocations newly formed during cool-down of the composite from processing temperatures increases with decreasing particle size. Therefore the number of obstacles for the dislocation motion increases and the stress necessary for the motion of dislocations increases, too. The difference in CTE between the matrix and the particle is decreasing from Mg/Al_2O_3 through Mg/Y_2O_3 to Mg/ZrO_2. It should be mentioned that the effect of different types of nanoparticles on the yield stress is attributed not only to the CTE difference but also to the properties of the matrix/particle interface. The bonding between the particles and Mg matrix influences also the deformation behaviour. The contribution to the yield stress owing to Orowan mechanisms can be ignored since it is about one order of magnitude lower. Since grain size differences between materials presented in this work are small, the Hall-Petch relation is not considered. However, the Hall-Petch mechanism should be taken into account when the nanocomposites are compared with coarse grained magnesium.

It is obvious that the test temperature has a significant influence on the shape of the true stress-true strain curves that indicate a balance between hardening and softening at higher temperatures. The yield stress and maximum stress decrease rapidly with temperature. This indicates the occurrence of thermally activated processes. It should be mentioned that five independent slip systems are necessary for deformation of polycrystals. The dominant slip mode in magnesium single crystals is basal slip. But there are only two independent slip systems. The activity of non-basal slip systems is therefore required. In magnesium the glide of dislocations in second-order pyramidal slip systems should be considered [34, 35]. The activity of pyramidal slip systems increases with increasing temperature. Interactions between the basal dislocations (**a** dislocations) and the pyramidal (**c** + **a**) dislocations may result in creation of new basal dislocations [34, 36]. An interaction among the pyramidal (**c** + **a**) dislocations can result in softening because annihilation of dislocations may occur. The observed macroscopic work hardening rate is a sum of hardening and softening mechanisms. We assume that cross slip of screw dislocation segments of both (**c** + **a**) and **a** dislocations is softening mechanism. The stress necessary for cross slip of dislocations decreases rapidly with temperature. A relative large elongation to failure observed in experiment also indicates the activity of (**c** + **a**) dislocations and the interactions between **a** and (**c** + **a**) dislocations. The different deformation behaviours of materials are very probably also influenced by the bonding between matrix and ceramic particles, as will be discussed below.

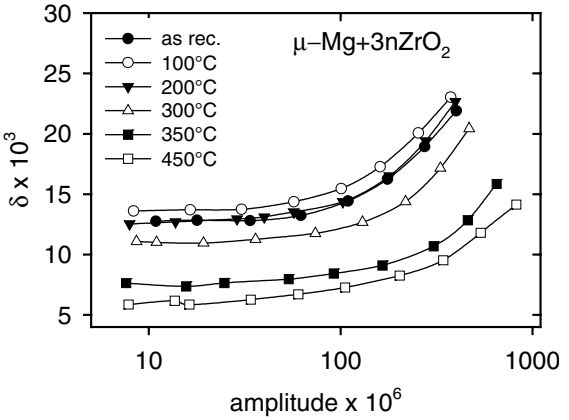

Fig. 6. Strain amplitude dependence of the logarithmic decrement for microcrystalline Mg reinforced with 3 vol.% of ZrO_2 nanoparticles annealed at various temperatures.

3.2. Damping in microcrystalline and nanocrystalline Mg

Figure 6 shows the logarithmic decrement, δ, plotted against the logarithm of the maximum strain amplitude, ε, for μ-Mg+3n-ZrO_2 [21, 25]. The δ values were measured before (as-received) and after step by step annealing at increasing upper temperature of the cycle. The measured δ-ε dependence exhibits two regions and can be expressed as

$$\delta(\varepsilon) = \delta_0 + \delta_{\mathrm{H}}(\varepsilon), \tag{4}$$

where δ_0 is the amplitude independent component found at lower strain amplitudes. For higher strain amplitudes, the component $\delta_{\mathrm{H}}(\varepsilon)$ increases with increasing strain amplitude. Similar dependences were observed for Mg-based composites [37, 38]. In the case of the μ-Mg+3n-ZrO_2 composite, the thermal treatment influences mainly δ_0 component of the decrement. It is important to note that very high values of damping in the amplitude independent component – in order of 10^{-2} – were obtained.

The strain amplitude dependences of δ for μ-Mg+3n-Al_2O_3 are given in Fig. 7 [21]. In the contrast to μ-Mg+3n-ZrO_2, the thermal cycling of μ-Mg+3n-Al_2O_3 influences mainly the δ_{H} component that increases with increasing upper temperature of the cycle. Trojanová et al. [39] could show that the values of δ for μ-Mg+1n-Al_2O_3 (12 nm) composite are significantly higher than those for unreinforced microcrystalline Mg. While changes in the δ values for Mg without nanoparticles are very small in the temperature range from 100 to 450 ℃, the δ_{H} component of the composite increases with increasing temperature, which may be explained by thermal stresses in the composite material. It is generally accepted that the δ_0 component is connected with the material mi-

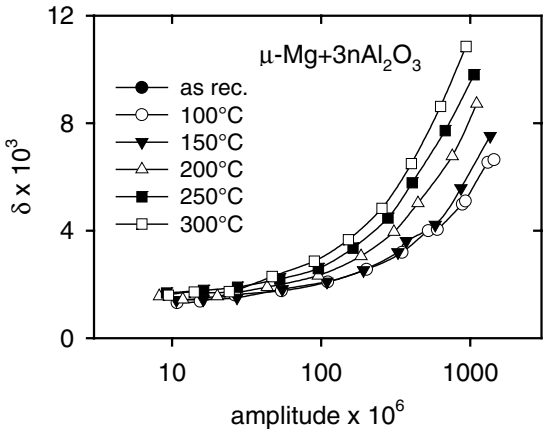

Fig. 7. Strain amplitude dependence of the logarithmic decrement for microcrystalline Mg reinforced with 3 vol.% of Al_2O_3 nanoparticles; annealed at various temperatures.

crostructure and the amplitude dependent component δ_H is due to an interaction of dislocations with point defects (e.g. solute atoms or their clusters, small particles). The newly formed dislocations due to the CTE difference (Eq. (3)) may be sources of a higher damping owing to the motion of vibrating dislocations under cyclic loading.

According to the Granato-Luecke theory [40], weak and strong pinning points restrict motion of dislocations in their glide plane. L_N and ℓ are the mean distances between strong pinning points and that between weak points, respectively. At higher strain amplitudes, the force exerted on dislocation at the weak pinning points becomes higher than the binding force. The dislocation segments break away from some weak pinning points within L_N. This leads to a drastic instantaneous increase in the dislocation strain and thus giving rise to a high level of the logarithmic decrement. We assume that the mean distance between weak pinning points $\ell < L_N$, and the mean total density of dislocations is ρ. The breakaway stress decreases with increasing temperature. The breakaway process is thermally activated. The stress dependence of the component δ_H can be expressed as

$$\delta_H = \frac{\rho L_N^2}{6}\,\frac{\nu}{\omega}\left(\frac{3\pi kT}{2U_0}\right)^{1/2}\left(\frac{\ell^3\sigma_0^2}{U_0 G}\right)^{1/2}\times \\ \times \exp\left[-\frac{4}{3}\,\frac{U_0}{kT}\left(\frac{U_0 G}{\ell^3}\right)^{1/2}\frac{1}{\sigma_0}\right], \qquad (5)$$

where U_0 is the activation energy, G is the shear modulus, ν is the attempt dislocation frequency, σ_0 is the amplitude of the applied stress and ω is its frequency, k is the Boltzmann constant and T is temperature. The maximum strain amplitude ε_0 is proportional to σ_0. Equation (5) may be rewritten in the form $\delta_H = C_1\varepsilon\exp(-C_2/\varepsilon)$ that can be used to analyse the experimental data. It is obvious that the value of the C_2 parameter decreases with increasing temperature and the value of the C_1 parameter increases with increasing temperature of thermal cycling (heating). But the exponential term increases with increasing temperature. This leads to the observed increase in the amplitude dependent decrement component. The C_1 parameter is proportional to $\ell^{3/2}$ and the C_2 is proportional to $\ell^{-3/2}$ and thus, the experimental data indicate that the length of the dislocation segments between weak pinning points could increase with increasing upper temperature. This may be explained assuming that during thermal cycling, new dislocations are created due to the CTE difference (Eq. (3)). While the number of weak pinning points remains constant, the mean length of dislocation segments between weak pinning points increases effectively and hence the δ_H component should increase, which is observed. The higher temperature of the cycling, the higher dislocation density and the higher increase in the effective length of the ℓ segments.

The contribution of interfaces to internal friction depends on the character of interfacial bonding. The internal friction of a composite with the perfectly bonded interface depends on the shape of particles, their volume fraction and the magnitude of local stress at the particle-matrix interface [41, 42]. In the case of weak bonding at the interface, interfacial slip (sliding at the interface) may occur. Then, the frictional energy loss caused by the sliding at interfaces may become a primary source of damping [41, 42].

Very high values of δ_0 for microcrystalline and nanocrystalline magnesium reinforced by zirconia nanoparticles and carbon particles are very probably caused by interfacial slip (sliding) due to weak bonding between particles and matrix. High values of δ_0 obtained for microcrystalline and ultrafine-grained Mg are very probably caused by grain boundary sliding supported by diffusion processes.

4. Conclusions

The deformation behaviour and damping of magnesium-based nanocomposites depend on the kind of nanoparticles and on the grain size. Ceramic and graphite nanoparticles in magnesium matrix significantly increase the yield stress and the maximum stress at room temperature. The yield stress and the maximum stress decrease rapidly with increasing temperature. Al_2O_3 particles are most effective in increasing the strength properties whereas ZrO_2 nanoparticles are most effective in increasing ductility. An increase in the dislocation density due to the difference in CTE between magnesium and nanoparticles is responsible for an increase in the yield stress at room temperature.

The dependence of the yield stress on the particle size may be explained by an increase of the newly formed dislocations, the density of which increases with a decrease in the particle size. The shape of the true stress--true strain curves at higher temperatures indicates a dynamic balance between hardening and softening. The motion of dislocations in non-basal slip systems, including cross slip, is the main thermally activated process causing softening.

The nanoparticles influence the amplitude independent component of the logarithmic decrement. The ZrO_2 nanoparticles influence the decrement more than the Al_2O_3 nanoparticles. The thermal treatment (thermal cycling) influences the value of the logarithmic decrement.

Acknowledgements

The authors acknowledge support of this work by the Grant Agency of the Czech Republic under grant 106/06/1354.

References

[1] POLMEAR, J. J.: Mater. Sci. Tech., *10*, 1994, p. 1.
[2] LUO, A.—PEKGULERYUZ, M. O.: J. Mater. Sci., *29*, 1994, p. 5259.
[3] JÄGER, A.—LUKÁČ, P.—GÄRTNEROVÁ, V.: Kovove Mater., *42*, 2004, p. 165.
[4] TROJANOVÁ, Z.—LUKÁČ, P.: Kovove Mater., *43*, 2005, p. 73.
[5] TROJANOVÁ, Z.: Kovove Mater., *43*, 2005, p. 182.
[6] NIE, J. F.—MUDDLE, B. C.: Acta Mater., *48*, 2000, p. 1691.
[7] ANDERSSON, P.—CÁCERES, C. H.—KOIKE, J.: Mater. Sci. Forum, *419–422*, 2003, p. 123.
[8] ONO, N.—NAKAMURA, K.—MIURA, S.: Mater. Sci. Forum, *419–422*, 2003, p. 195.
[9] SOMEKAWA, H.—MUKAI, T.: Scripta Mater., *53*, 2005, p. 1059.
[10] SU, C. W.—CHUA, B. W.—LU, L.—LAI, M. O.: Mater. Sci. Eng. A, *402*, 2005, p. 163.
[11] HALL, E. O.: Proc. Phys. Soc. London B, *64*, 1951, p. 747.
[12] PETCH, N. J.: J. Iron Steel Inst., *174*, 1953, p. 25.
[13] HWANG, S.—NISHIMURA, C.—McCORMICK, P. G.: Scripta Mater., *44*, 2001, p. 1507.
[14] SURYANARAYANA, C.: Adv. Eng. Mater., *7*, 2005, p. 983.
[15] OAKLAY, R.—COCHRANE, R. F.—STEVENS, R.: Key Eng. Mater., *104–107*, 1995, p. 387.
[16] YE, H. Z.—LIU, X. Y.: J. Mater. Sci., *39*, 2004, p. 6153.
[17] LUKÁČ, P.—TROJANOVÁ, Z.—CHMELÍK, F.—RUDAJEVOVÁ, A.: Int. J. Mater. Product. Tech., *18*, 2003, p. 57.
[18] NASER, J.—RIEHEMANN, W.—FERKEL, H.: Mater. Sci. Eng. A, *234–236*, 1997, p. 467.
[19] NASER, J.—FERKEL, H.—RIEHEMANN, W.: Mater. Sci. Eng A, *234–236*, 1997, p. 470.
[20] LEE, C. J.—HUANG, J. C.—HSIEH, P. J.: Scripta Mater., *54*, 2006, p. 1415.
[21] LUKÁČ, P.—TROJANOVÁ, Z.: Int. J. Mater. Product. Tech., *23*, 2005, p. 21.
[22] LUKÁČ, P.—TROJANOVÁ, Z.—SZÁRAZ, Z.—SVOBODA, M.—FERKEL, H.: Z. Metallkde, *97*, 2006, p. 344.
[23] NOWICK, A. S.—BERRY, B. S.: Anelastic Relaxation in Crystalline Solids. New York, Academic Press 1972.
[24] FERKEL, H.: Adv. Eng. Mater., *5*, 2003, p. 886.
[25] TROJANOVÁ, Z.—FERKEL, H.—LUKÁČ, P.—RIEHEMANN, W.: Phys. Stat. Sol., *193*, 2002, p. 205.
[26] TROJANOVÁ, Z.—LUKÁČ, P.—SZÁRAZ, Z.: Rev. Adv. Mater. Sci., *10*, 2005, p. 437.
[27] TROJANOVÁ, Z.—DROZD, Z.—LUKÁČ, P.—MÁTHIS, K.—FERKEL, H.—RIEHEMANN, W.: Scripta Mater., *42*, 2000, p. 1085.
[28] FERKEL, H.—MORDIKE, B. L.: Mater. Sci. Eng. A, *298*, 2001, p. 193.
[29] HASSAN, S. F.—GUPTA, M.: Mater. Sci. Eng. A, *392*, 2005, p. 163.
[30] HASSAN, S. F.—GUPTA, M.: Mater. Sci. Eng. A, *425*, 2006, p. 22.
[31] HASSAN, S. F.—GUPTA, M.: J. Mater. Sci., *41*, 2006, p. 2229.
[32] ARSENAULT, J. R.—SHI, N.: Mater. Sci. Eng., *81*, 1986, p. 175.
[33] DUNAND, D. C.—MORTENSEN, A.: Acta Metall. Mater., *39*, 1991, p. 127.
[34] LUKÁČ, P.: Czech. J. Phys. B, *31*, 1981, p. 135.
[35] AGNEW, S. R.—HORTON, J. A.—YOO, M. H.: Metall. Mater. Trans. A, *33*, 2002, p. 851.
[36] LUKÁČ, P.—MÁTHIS, K.: Kovove Mater., *40*, 2002, p. 281.
[37] TROJANOVÁ, Z.—LUKÁČ, P.—RIEHEMANN, W.—MORDIKE, B. L.: Mater. Sci. Eng. A, *324*, 2002, p. 122.
[38] TROJANOVÁ, Z.—LUKÁČ, P.—RUDAJEVOVÁ, A.: Mater. Sci. Eng. A, *370*, 2004, p. 542.
[39] TROJANOVÁ, Z.—LUKÁČ, P.—FERKEL, H.—MORDIKE, B. L.—RIEHEMANN, W.: Mater. Sci. Eng. A, *234–236*, 1997, p. 798.
[40] GRANATO, A. V.—LUECKE, K.: J. Appl. Phys., *52*, 1981, p. 7136.
[41] ZHANG, J.—PEREZ, R. J.—LAVERNIA, E. J.: Acta Metall. Mater., *42*, 1994, p. 395.
[42] ZHANG, J.—PEREZ, R. J.—WONG, C. R.—LAVERNIA, E. J.: Mater. Sci. Eng. R, *13*, 1994, p. 325.